IJMMM International Journal of Minerals, Metallurgy and Materials 矿物冶金与材料学报（英文版）

Two new amino acid derivatives as green corrosion inhibitors against Q235 steel in HCl solution: Experimental and theoretical investigations

Chaoyi Li, Minghao Su, Tianyi Hou, Yuhe Shi, Junrong Huang, Jing Qing, Wenxin Niu, Yinghe Zhang, Ling Zhang, and Hengzhi You

Cite this article as:
Chaoyi Li, Minghao Su, Tianyi Hou, Yuhe Shi, Junrong Huang, Jing Qing, Wenxin Niu, Yinghe Zhang, Ling Zhang, and Hengzhi You, Two new amino acid derivatives as green corrosion inhibitors against Q235 steel in HCl solution: Experimental and theoretical investigations, *Int. J. Miner. Metall. Mater.*, 32(2025), No. 7, pp. 1617-1627. https://doi.org/10.1007/s12613-024-3011-8

Articles you may be interested in

L. K. M. O. Goni, M. A. Jafar Mazumder, S. A. Ali, M. K. Nazal, and H. A. Al-Muallem, Biogenic amino acid methionine-based corrosion inhibitors of mild steel in acidic media, *Int. J. Miner. Metall. Mater.*, 26(2019), No. 4, pp. 467-482. https://doi.org/10.1007/s12613-019-1754-4

Milad Edraki and Davood Zaarei, Azole derivatives embedded in montmorillonite clay nanocarriers as corrosion inhibitors of mild steel, *Int. J. Miner. Metall. Mater.*, 26(2019), No. 1, pp. 86-97. https://doi.org/10.1007/s12613-019-1712-1

Uttam Bhandari, Congyan Zhang, Shengmin Guo, and Shizhong Yang, First-principles study on the mechanical and thermodynamic properties of MoNbTaTiW, *Int. J. Miner. Metall. Mater.*, 27(2020), No. 10, pp. 1398-1404. https://doi.org/10.1007/s12613-020-2077-1

Akhya kumar Behera, Amlan Das, Sanjeev Das, and Archana Mallik, Electrochemically functionalized graphene as an anti-corrosion reinforcement in Cu matrix composite thin films, *Int. J. Miner. Metall. Mater.*, 28(2021), No. 9, pp. 1525-1533. https://doi.org/10.1007/s12613-020-2124-y

Bao Liu, Shuo Wang, Cheng-yan Wang, Bao-zhong Ma, and Yong-qiang Chen, Electrochemical behavior and corrosion resistance of IrO_2–ZrO_2 binary oxide coatings for promoting oxygen evolution in sulfuric acid solution, *Int. J. Miner. Metall. Mater.*, 27(2020), No. 2, pp. 264-273. https://doi.org/10.1007/s12613-019-1847-0

Shuang-yu Cai, Lei Wen, and Ying Jin, A comparative study on corrosion kinetic parameter estimation methods for the early stage corrosion of Q345B steel in 3.5wt% NaCl solution, *Int. J. Miner. Metall. Mater.*, 24(2017), No. 10, pp. 1112-1124. https://doi.org/10.1007/s12613-017-1502-6

IJMMM WeChat

QQ author group

INTERNATIONAL JOURNAL OF
Minerals, Metallurgy and Materials

Volume 32, Number 7, July 2025
Page 1617

Research Article https://doi.org/10.1007/s12613-024-3011-8

Two new amino acid derivatives as green corrosion inhibitors against Q235 steel in HCl solution: Experimental and theoretical investigations

Chaoyi Li[1),*], *Minghao Su*[1),*], *Tianyi Hou*[1)], *Yuhe Shi*[1)], *Junrong Huang*[1)], *Jing Qing*[2)], *Wenxin Niu*[3)], *Yinghe Zhang*[1),✉], *Ling Zhang*[1),✉], *and Hengzhi You*[1),✉]

1) School of Science, Harbin Institute of Technology (Shenzhen), Shenzhen 518055, China
2) Shenzhen Zhonghe Headway Bio-Sci & Tech Co., Ltd., Shenzhen 518055, China
3) State Key Laboratory of Electroanalytical Chemistry, Changchun Institute of Applied Chemistry, Chinese Academy of Sciences, Changchun 130022, China
(Received: 12 March 2024; revised: 13 September 2024; accepted: 18 September 2024)

Abstract: Amino acids have emerged as promising green alternatives to replace toxic inhibitors in corrosion protection applications. In this study, we present a one-step synthetic approach to get 4-(tert-butyl)benzoyl)methionine (P-Meth) and 4-(tert-butyl)benzoyl)cysteine (P-Cys) through the acylation reactions between methionine or cysteine and p-tert-butylbenzoic acid, respectively, which exhibit a super protective performance toward metals against corrosion. The corrosion rates of Q235 steel in 1 M HCl were reduced from 4.542 to 0.202 and 0.312 mg·h^{-1}·cm^{-2} in the presence of 100 mg·L^{-1} P-Meth and P-Cys, respectively. The surface structures of Q235 steel remained unbroken after 12 h in 1 M HCl medium. The charge transfer resistances of corrosion reactions were enhanced by 12 and 9 times in the presence of P-Meth and P-Cys, respectively. P-Meth and P-Cys were adsorbed onto the Q235 steel via chemical actions, which were accompanied by minimal physical action. Molecular dynamic simulations demonstrate the higher binding energy of P-Meth onto Q235 steel than P-Cys. The study contributes to the corrosion protection of metals with green and environmentally friendly methods.

Keywords: amino acid derivatives; anti-corrosion reagents; green chemistry; Q235 steel; density functional theory

1. Introduction

Corrosion inhibitors have gained prominence as a burgeoning and extensively embraced approach for the prevention of metal corrosion owing to their practicality and economic viability [1–2]. A heightened focus has been allotted to the development of environmentally friendly corrosion inhibitors, which is driven by the increased emphasis on environmental protection and the need for cost-effective solutions [3]. Numerous ecofriendly organic inhibitors, including carbohydrates [4], lignin [5], ionic liquids [6], expired drugs [7], and amino acids [8–10], have been reported. However, their practical application in the industry poses challenges. The extraction process of carbohydrates and lignin is laborious [11], and the synthesis of ionic liquids typically involves multistep procedures, which results in elevated costs [12]. By contrast, their abundant natural availability, low toxicity, and excellent solubility make amino acids as the ideal inhibitor materials.

Amino acids exhibit a notable corrosion-inhibiting effect primarily at high concentrations, which were usually used as the specific additives [13–17]. Electrochemical and computational analysis were conducted in 1 M HCl containing 0.01 M cysteine, L-Histidine, L-Tryptophan, and L-Serine for the corrosions of mild steel, and the inhibition efficiencies (IE) were 85.1%, 93.4%, 96.3%, and 45.1%, respectively [18]. It suggested that abundant active atoms such as N and S benefited to promote the protective abilities. Amino acids inherently possess carboxyl and amino groups, with some featuring heteroatoms (i.e., O, S, and N) or conjugated structures and can be easily functionalized. Encouragingly, modifications such as varying the length of the carbon skeleton [19], incorporating heterocycles and heteroatoms [20–21], and attaching polar groups [22] to amino acids enhance their anticorrosion performance. These insights substantially informed our work, which indicates that the chemical modification of amino acids represents a viable and efficient approach to achieve the outstanding IE and develop environmentally friendly corrosion inhibitors.

Methionine and cysteine are distinguished by their –SCH_3 or –SH groups, serving as excellent centers for the adsorptions on metal surfaces [23]. However, their satisfactory anticorrosion efficiency is only achievable at relatively high concentrations [24]. In this study, to increase the corrosion inhibition performance of these natural products, we conducted acylation reactions to functionalize methionine and cysteine

*These authors contributed equally to this work.

✉ Corresponding authors: Yinghe Zhang E-mail: zhangyinghe@hit.edu.cn; Ling Zhang E-mail: zhangling2018@hit.edu.cn; Hengzhi You E-mail: youhengzhi@hit.edu.cn

with p-tert-butylbenzoic acid, which resulted in the formation of derivatives referred to as 4-(tert-butyl)benzoyl)methionine (P-Meth) and 4-(tert-butyl)benzoyl)cysteine (P-Cys), respectively. Subsequently, we assessed the corrosion inhibition performance of these amino acid derivatives on Q235 steel in 1 M HCl. The performances of the corrosion inhibitors were investigated via the weight-loss analysis, electrochemical impedance spectroscopy (EIS), and potentiodynamic polarization analysis. The morphologies of Q235 steels were not changed in 1 M HCl containing P-Meth and P-Cys according to the scanning electron microscopy (SEM) characterizations. In addition, adsorption isotherm modeling, quantum chemistry calculations, density functional theory (DFT), and molecular dynamics (MD) simulations were employed to comprehensively explore the corrosion inhibition performance of these molecules from various perspectives.

2. Experimental

2.1. Chemicals and material preparation

Hydrochloric acid (analytical reagent (AR), 37%wt%), ethyl acetate (EA, AR, ≥99.5wt%), dichloromethane (DCM, AR, ≥99.5wt%), chloroform-d (AR, 98wt%), and methyl alcohol (MeOH, AR, ≥99.5wt%) were purchased from Adamas company. L-methionine (99wt%), L-cysteine (99wt%), and 4-tert-butylbenzoyl chloride (98wt%) were purchased from Energy Chemical company. Q235 steel samples (containing 0.13wt% C, 0.032wt% Si, 0.58wt% Mn, 0.035wt% P, 0.035wt% S, 0.15wt% Cr, 0.13wt% N, 0.15wt% Cu, etc.) were purchased from a water treatment company. 1 M HCl was applied as the electrolyte to simulate the acidic environments. The concentrations of synthetic corrosion inhibitors were 25–100 mg·L^{-1} in the electrolytes. The solutions of corrosion inhibitors were prepared by dissolving the powders in ethanol, which were diluted in 1 M HCl for the further use.

2.2. Instruments

SEM characterizations were performed using SU8010 instruments. Electrochemical impedance spectra (EIS) and potentiodynamic polarizations were got on the CHI 760E electrochemical workstation (China). The proton (^{1}H) and carbon (^{13}C) nuclear magnetic resonance (NMR) spectra were recorded using Quantum-I 400M spectrometer from Q.One Instruments. Column chromatography purifications were performed by flash chromatography using Merck silica gel 60.

2.3. Synthesis of amino acid derivatives

In our work, two amino acid derivatives (P-Meth and P-Cys) were synthesized following condensation reactions (Fig. 1). First, methionine (0.75 g, 5 mmol) was added to a 50 mL round-bottomed flask containing 2 M NaOH aqueous solution (0.4 g, 10 mmol) in an ice bath. Then, 4-tert-butylbenzoyl chloride (0.98 mL, 5 mmol) was added dropwise to the solution, and the resulting mixture was continuously stirred for 24 h at room temperature (r.t.). After the reactions, the pH was adjusted to 1–2 using diluted HCl. Then, the aqueous phase was extracted several times using EA, and the organic phase was collected and dried using anhydrous magnesium sulfate. The solvent was evaporated, and the mixture was purified via column chromatography (volume ratio of DCM to MeOH, 9:1) to obtain P-Meth (1.17 g, yield, 76%). P-Cys (1.02 g, yield, 73%) was synthesized through a similar method, except that cysteine (0.60 g, 5 mmol) was used to replace methionine.

2.4. Structure characterizations of corrosion inhibitors

The structures of P-Meth and P-Cys were analyzed by ^{1}H NMR and ^{13}C NMR. The chemical shifts (δ) were reported in parts per million (ppm) with tetramethylsilane as 0 ppm. Coupling constants (J) were reported in Hertz (Hz). The residual solvent peaks for chloroform-d were used as the internal references, which appeared at δ 7.26 and δ 77.0 in ^{1}H NMR and ^{13}C NMR spectra, respectively (Figs. S1–S4). Solvents were freshly dried and degassed prior to use.

2.5. Weight-loss measurements

Weight-loss analysis was performed to assess the corrosion inhibition properties of the compounds [25]. Q235 steel samples (1.0 cm × 1.0 cm × 0.1 cm) were rinsed with ethanol and ultrapure water, dried in air, and weighed. Subsequently, the samples were immersed in 100 mL of 1 M HCl solution with or without P-Meth or P-Cys at a temperature of (25 ± 2)°C for 12 h. Following each experiment, the steel samples were withdrawn, rinsed with ultrapure water, dried, and reweighed to calculate the lost weights. This procedure was repeated thrice to obtain the average values of the lost weights.

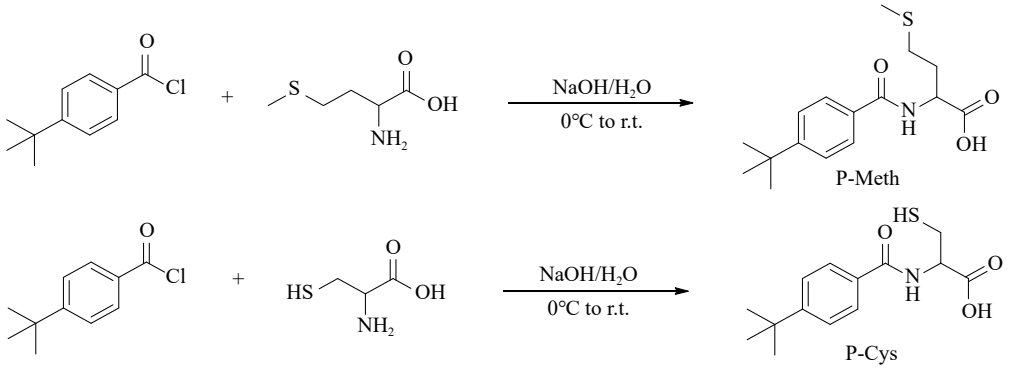

Fig. 1. Synthesis routes of P-Meh and P-Cys.

2.6. Electrochemical measurements

All electrochemical assessments, including EIS and potentiodynamic polarization curves, were conducted at a controlled temperature of (25 ± 2)°C. Q235 steel, which was encapsulated in Teflon to form electrodes with a 2 mm cross-sectional diameter, served as the working electrode. The three-electrode cell system comprised a Q235 steel electrode, a saturated calomel electrode, and a platinum electrode, which were used as the working, reference, and counter electrodes, respectively. Prior to the EIS, the steel electrodes were polished using SiC papers (800–1000 grit) and thoroughly rinsed with ethanol and ultrapure water before each use. The working electrodes were immersed into the electrolytes for 30 min per test to establish a stable open-circuit potential (OCP). EIS measurements were conducted in 100 kHz–0.01 Hz with the sinusoidal potential perturbation as 5 mV. The polarization curves were measured in the range of (OCP ± 250) mV at a scanning rate of 0.01 $mV \cdot s^{-1}$. Each experiment was performed thrice to get the average values.

2.7. Quantum chemical calculations

The molecular structures of P-Meth and P-Cys were optimized through DFT simulations with B3LYP hybrid functional and 6-31g(d, p) basis set in Gaussian 09 [26]. Subsequently, the pre-optimized geometry was used to calculate the single-point energy via the B3LYP/6-311g(d, p) method. Then, the quantum chemical parameters of P-Meth and P-Cys, including atomic charges, the energy state of highest occupied molecular orbital (E_{HOMO}), and the lowest occupied molecular orbital (E_{LUMO}), and Fukui functions were generated to analyze the interaction forces between the corrosion inhibitors and steel surfaces [27].

2.8. MD modeling

The interaction forces between P-Meth and P-Cys and steel surfaces were also investigated through MD modeling using the Materials Studio package [28–31]. To describe the corrosion process, we constructed a simulation box, which comprised a single inhibitor molecule, hydrogen and chlorine ions, a fixed Fe (110) surface, and the aqueous medium. MD simulation was started with geometric optimization and then run with a Compass II force field under 1.0 fs time step and 300 ps simulation period at 298 K [32]. In addition, Monte Carlo (MC) simulations were used to investigate the adsorption energies of inhibitor molecules and Fe (110) under vacuum conditions.

3. Results and discussion

3.1. Weight-loss and surface morphology analysis

The inhibition effects of P-Meth and P-Cys on Q235 steel in 1 M HCl solution were initially investigated through the weight-loss analysis. From Eqs. (1)–(3), we can obtain the surface coverage ratios for P-Meth and P-Cys.

$$v = \frac{w_0 - w}{S \cdot t} \tag{1}$$

$$\mathrm{IE} = \frac{v_0 - v}{v_0} \times 100\% \tag{2}$$

$$\theta = \frac{v_0 - v}{v_0} \tag{3}$$

where w_0 and w are the weights of steels before and after corrosions (mg); S is the surface area of steels (cm^2); t is the immersion time (h); v_0 and v are the corrosion rates without and with corrosion inhibitors ($mg \cdot h^{-1} \cdot cm^{-2}$); θ is the surface coverage ratio of corrosion inhibitors.

The corrosion rates and inhibition efficiencies of Q235 steel in 1 M HCl solution and surface coverage ratios in the presence of different concentrations (c, $mg \cdot L^{-1}$) of corrosion inhibitors were shown in Table 1. In the absence of P-Meth or P-Cys, the corrosion rates were measured to be 4.542 $mg \cdot h^{-1} \cdot cm^{-2}$ in 12 h. With P-Meth or P-Cys in HCl mediums, the corrosion rates were decreased a lot. When the concentrations of P-Meth or P-Cys were increased to 100 $mg \cdot L^{-1}$, the corrosion rates were down to 0.202 and 0.312 $mg \cdot h^{-1} \cdot cm^{-2}$ in 12 h. The inhibition performance of P-Meth was better than that of P-Cys. When 25 $mg \cdot L^{-1}$ P-Meth was added, the inhibition efficiencies were high as 83.03%, and increased to 94.38% when the concentration of P-Meth was increased to 75 $mg \cdot L^{-1}$. The corrosion rate, inhibition efficiencies, and surface coverage ratios were not increased remarkably when the concentrations of P-Meth was increased from 75 to 100 $mg \cdot L^{-1}$, indicating that 75 $mg \cdot L^{-1}$ P-Meth in 1 M HCl were enough to protect Q235 steels from corroding, and the steel surfaces were fully covered by P-Meth in this condition ($\theta = 0.9555$).

Table 1. Corrosion rates and inhibition efficiencies of Q235 steel in 1 M HCl solution and surface coverage ratios in the presence of different concentrations of corrosion inhibitors

Inhibitor	c / ($mg \cdot L^{-1}$)	v / ($mg \cdot h^{-1} \cdot cm^{-2}$)	IE / %	θ	SD[a]
Blank	—	4.542	—	—	—
P-Meth	25	0.771	83.03	0.8303	0.034
	50	0.565	87.56	0.8756	0.051
	75	0.255	94.38	0.9438	0.027
	100	0.202	95.55	0.9555	0.021
P-Cys	25	2.056	54.73	0.5473	0.038
	50	1.225	73.03	0.7303	0.013
	75	0.553	87.82	0.8782	0.024
	100	0.312	93.13	0.9313	0.017

Note: SD[a]—Standard deviations.

Conversely, the inhibition performances of P-Cys were gradually improved with the concentration increased gradually. At 100 $mg \cdot L^{-1}$, the P-Cys corrosion rates were reached to minimum values, and the inhibition efficiencies and the sur face coverage ratios of inhibitors reached to the maximum values (IE = 93.13, $\theta = 0.9313$). Thus, good protective performances were achieved by the two kinds of amino acid derivatives, and 100 ppm were enough to keep the steel surfaces from corroding. The inhibitors containing $–SCH_3$ showed better protective effects than those with –SH, indicating proper structures were very important to the adsorptions of

inhibitors onto the steel surfaces. Also, other heteroatoms such as N and O, π-electrons, and carboxylic acid anions were also important to the protective effects of inhibitors.

The surface morphology of Q235 steel was analyzed via SEM characterizations (Fig. 2). The Q235 steel surface was flat, and horizontal polished scars were clearly visible prior to corrosion (Fig. 2(a), boxed area). After the corrosions in 1 M HCl solution for 12 h, the polished surfaces of Q235 steels were considerably damaged, and severe corrosion traces and many irregular grooves were observed (Fig. 2(b), boxed area). In contrast, in 1 M HCl medium containing 100 mg·L^{-1} of either P-Meth or P-Cys, the steel surfaces were kept well, and there were clear horizontal polished scars observed (Fig. 2(c) and (d)). Although subtle corrosion occurred along the horizontal scars, the polished surface was largely preserved. The results demonstrate that P-Meth and P-Cys exhibited remarkable corrosion inhibition performances in the acidic medium.

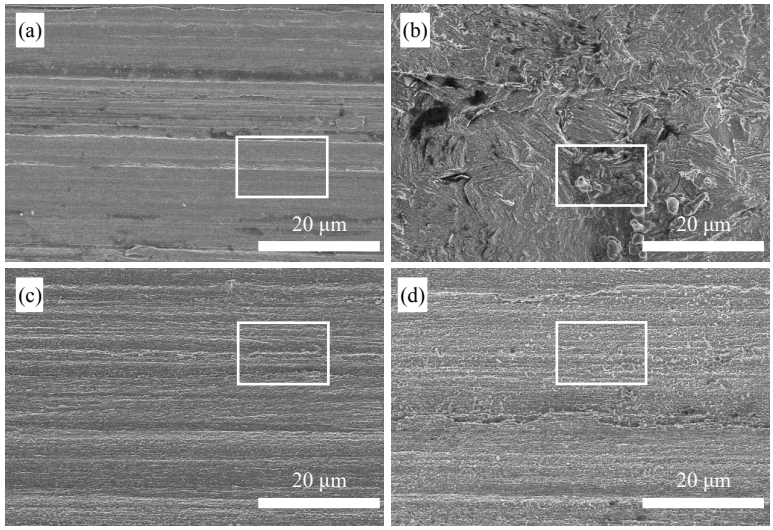

Fig. 2. SEM images of Q235 steels: (a) before corrosion; after corrosions in (b) 1 M HCl, (c) 1 M HCl with 100 mg·L^{-1} P-Meth, and (d) 1 M HCl with 100 mg·L^{-1} P-Cys.

3.2. EIS analysis

EIS analysis of Q235 steel electrodes were performed in HCl solutions with varying concentrations of P-Meth or P-Cys. All the Nyquist plots of the tested Q235 steel electrodes exhibited semicircles centered on the real axis, indicating the currents were controlled by the charge transfers and electrical double-layer capacitor (Fig. 3(a) and (b)). Notably, the alterations of P-Meth and P-Cys concentrations did not significantly alter the shapes of the semicircle, which indicated that the charge transfer mechanisms predominantly governed the corrosion processes of Q235 steel in 1 M HCl [33]. Contrastingly, with the concentrations of P-Meth and P-Cys increased, the charge transfer resistances (R_{ct}) were increased remarkably, demonstrating the good protecting abilities of P-Meth and P-Cys to Q235 steel electrodes in the strong acid solutions. The increased concentration of P-Meth and P-Cys led to the reduced number of corrosion sites on Q235 steel surfaces, which inhibited the corrosions via the augmentation of the surface coverages of adsorbed anti-corrosion molecules in the membranes [34].

The bode and phase-angle diagrams of P-Meth and P-Cys are shown in Fig. 3(c) and (d). The phase angles increased significantly through the additions of various concentrations of corrosion inhibitors. We attributed this outcome to the adsorption of inhibitors. In such a case, the corrosion reactions on steel surfaces were slowed down, and the dispersion effects were enhanced [35–36]. The low-frequency impedance modulus of $|Z|$ served as an important indicator of corrosion inhibition efficiencies, with high $|Z|$ values corresponding to the high corrosion inhibition efficiency. For the Q235 steel electrode in HCl solutions containing P-Meth and P-Cys, the low-frequency impedance modulus of $|Z|$ increased with their concentrations. The phase-angle plots revealed that with the increase in P-Meth and P-Cys concentrations in the medium frequency (f) range, the phase angle gradually increased, and the inhibition behaviors were improved. The findings indicated that at high concentrations of P-Meth and P-Cys, a high number of inhibitor molecules were adsorbed on Q235 steel surfaces [37].

The EIS results were excellently fitted to the equivalent circuit diagrams in Fig. 4. The calculations of double-layer capacitance (C_{dl}) were shown by Eqs. (4) and (5) [38]. The corrosion inhibition efficiencies can be also obtained via the EIS methods (Eqs. (6) and (7)).

$$Z_{CPE} = Y_0^{-1}(j\omega)^{-n} \tag{4}$$

$$C_{dl} = Y_0(\omega_{max})^{n-1} \tag{5}$$

$$R_p = R_f + R_{ct} \tag{6}$$

$$\eta_E = \frac{R_p - R_p^0}{R_p} \tag{7}$$

where Y_0, ω, j, and n represent the constant of constant phase element (CPE), angular frequency constant, imaginary constant, and empirical exponent, respectively (when $n = -1$, 0, 1, CPE represents the resistance, inductance, and pure capacitance, respectively). In addition, ω_{max} indicates the fre-

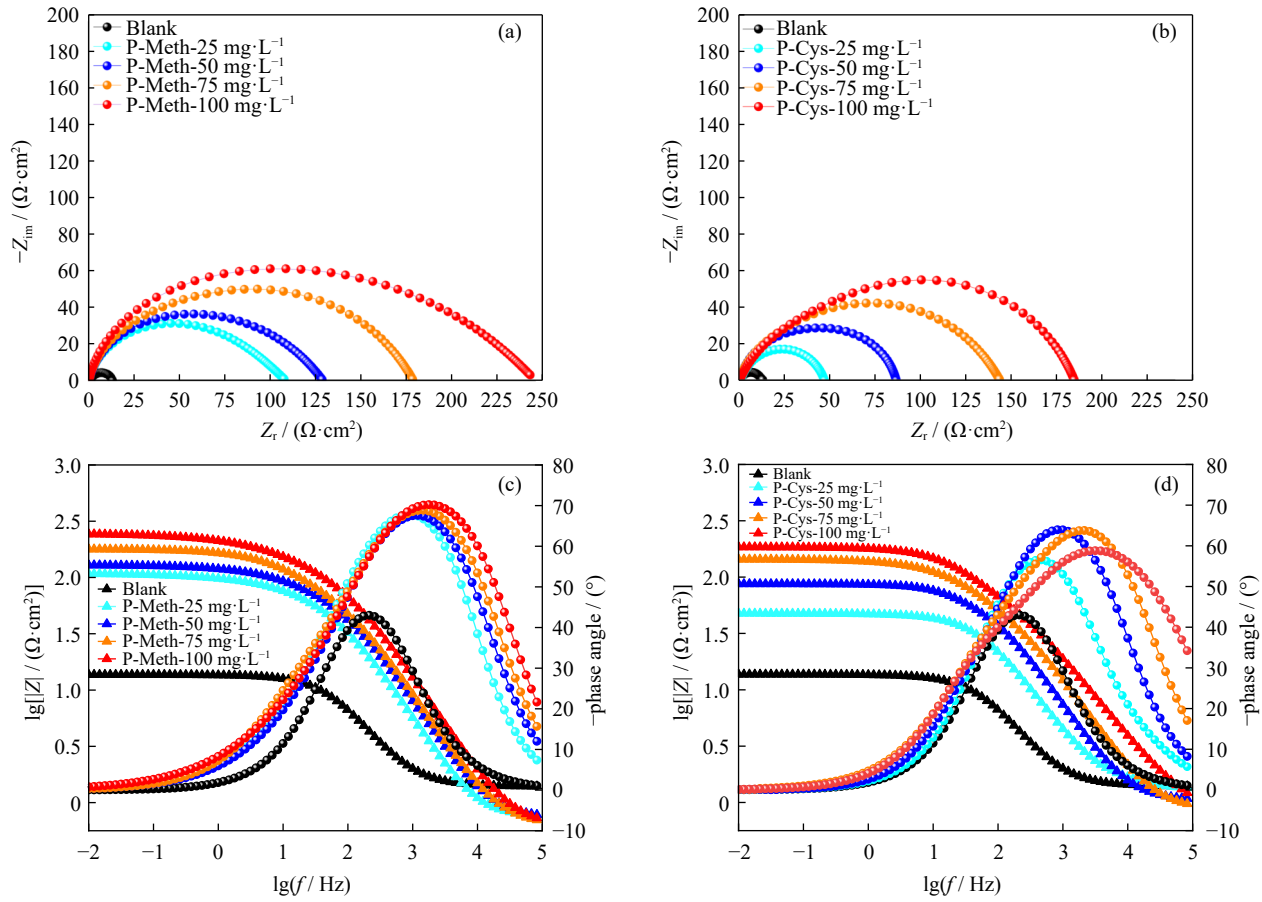

Fig. 3. (a, b) Nyquist and (c, d) bode plots of Q235 steel in 1 M HCl containing various concentrations of (a, c) P-Meth and (b, d) P-Cys.

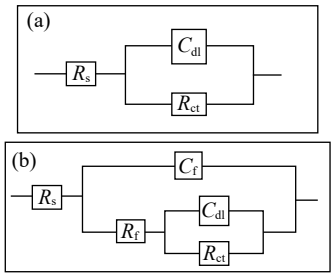

Fig. 4. Equivalent circuits of Q235 steel electrodes in the electrolytes (a) without and (b) with inhibitors. R_s, R_f, and C_f represent the solution resistance, thin-film resistance, and thin-film capacitance, respectively.

quency with the maximum value of virtual impedance. R_p and R_p^0 refer to the polarization resistance of electrolytes with and without corrosion inhibitors, respectively.

We obtained the impedance parameters from the fittings (Table 2). R_f exhibited a positive correlation with the corrosion inhibitor concentration, which increased a lot as the concentrations of inhibitors increased. Correspondingly, C_{dl} in the presence of P-Meth (25–75 mg·L^{-1}) and P-Cys (25–100 mg·L^{-1}) were lower than those without the inhibitors, indicating the low electronic conductivities of electrolytes in the presence of inhibitors. Moreover, C_f had a negative correlation with the inhibitor concentration. The decrease in C_f was attributed to the denser and thicker adsorption layer that formed on the metal surface, which was affected by the thickness of the protective layer or local dielectric constant [39–40]. Moreover, to highlight the improvement of the derivatives, we individually assessed the inhibition performance of the three precursors at a concentration of 50 mg·L^{-1}.

3.3. Potentiodynamic polarization analysis

Fig. 5 shows the potential polarization curves of Q235 steel immersed in various concentrations of P-Meth and P-Cys in a 1 M HCl solution at 25°C. When the inhibitor concentrations increased, the Tafel curves of the anode and cathode shifted toward a low current density. The minimum corrosion current density was observed at a concentration of 100 mg·L^{-1} for P-Meth and 100 mg·L^{-1} for P-Cys (Table 3). This result may be due to the adsorption and desorption of inhibitors during equilibrium at concentrations below 100 mg·L^{-1}. We surmised that the addition of P-Meth and P-Cys inhibited the anodic corrosion and cathode hydrogen evolution reaction of Q235 steel. Thus, P-Meth and P-Cys molecules acted as mixed-type corrosion inhibitors.

Table 3 contains the electrochemical parameters of corrosion potential (E_{corr}), corrosion current density (i_{corr}), anode and cathode Tafel slopes (β_a, β_c), and corrosion inhibition rate (η_{IE}, %). η_{IE} was calculated using Eq. (8):

$$\eta_{IE} = \frac{i_{corr}^0 - i_{corr}}{i_{corr}^0} \quad (8)$$

where i_{corr}^0 and i_{corr} represent the corrosion current density in

Table 2. Impedance parameters of P-Meth and P-Cys in 1 M HCl solution with various concentrations

Inhibitor	c / (mg·L^{-1})	R_s / (Ω·cm^2)	R_{ct} / (Ω·cm^2)	n_1	C_{dl} / (mF·cm^{-2})	R_f / (Ω·cm^2)	n_2	C_f / (mF·cm^{-2})	η_E / %	SD[a]	Chi-square, χ
Blank	—	1.3890	12.32	0.8288	653.5	—	—	—	—	—	7.9×10^{-4}
P-Meth	25	0.7563	78.09	0.4812	105.4	30.32	0.9158	58.02	88.63	3.1	1.7×10^{-3}
	50	0.733	69.73	0.5613	107.2	59.05	0.8809	55.81	90.43	2.8	4.6×10^{-4}
	75	0.6377	108.7	0.6403	568.5	69.79	0.8786	49.4	93.09	2.1	3.3×10^{-4}
	100	0.6261	161.4	0.5133	747.9	84.2	0.8806	33.84	94.98	2.3	6.3×10^{-4}
P-Cys	25	1.289	43.52	0.9628	12.54	2.783	0.7973	189.7	73.39	1.7	3.7×10^{-4}
	50	0.9265	28.3	0.9146	328.3	72.5	0.8316	77.08	87.78	2.2	1.9×10^{-3}
	75	0.8647	96.97	0.6316	345.1	46.39	0.8621	40.4	91.40	1.8	2.2×10^{-4}
	100	0.7543	123.9	0.7164	133.7	84.31	0.7712	54.35	94.08	2.3	4.9×10^{-4}

Note: SD[a]—Standard deviation of 3 independent measurements.

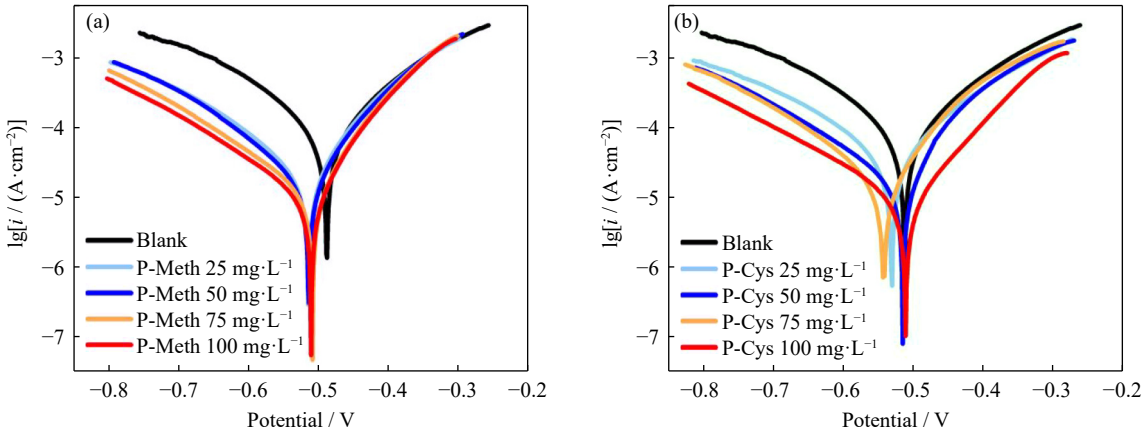

Fig. 5. Potentiodynamic polarization curves of Q235 steel in 1 M HCl containing different concentrations of (a) P-Meth and (b) P-Cys.

Table 3. Potentiodynamic polarization parameters of Q235 steel in 1 M HCl without or with different corrosion inhibitors

Inhibitor	c / (mg·L^{-1})	E_{corr} / mV	i_{corr} / (mA·cm^{-2})	$-\beta_c$ / (mV·dec^{-1})	β_a / (mV·dec^{-1})	η_{IE} / %	SD[a]
Blank	—	−484	68.61	7058	8066	—	—
P-Meth	25	−514	21.81	7546	10517	72.03	2.4
	50	−513	18.39	7836	11008	76.42	2.1
	75	−508	12.96	6851	12151	83.38	1.7
	100	−510	11.14	6636	12243	85.71	1.8
P-Cys	25	−504	39.89	6872	8471	48.85	2.1
	50	−490	19.76	7071	9989	74.47	2.2
	75	−515	16.77	7541	11324	78.50	1.9
	100	−486	9.64	6190	11942	88.30	1.6

Note: SD[a]—Standard deviation of 3 independent measurements.

the absence and presence of P-Meth or P-Cys, respectively.

The corrosion current density was substantially decreased with the addition of amino acid derivatives. This finding demonstrates the remarkable inhibition capabilities of these molecules. Depending on the displacement of the E_{corr} value, corrosion inhibitor molecules can be divided into anodic, cathode, and mixed types. Between the inhibited and uninhibited solutions, if the difference is greater than 85 mV, the amino acid derivatives can be identified as an anodic or cathodic inhibitor, and if the difference is less than 85 mV, the compound is considered a mixed-type inhibitor [41–43]. In this experiment, the maximum displacements of E_{corr} were 30 and 20 mV for P-Meth and P-Cys, respectively, which were less than 85 mV. This finding indicates that the two amino acid derivatives were mixed-type corrosion inhibitors. With the addition of the inhibitors, the corrosion potential became more negative, which demonstrates that both inhibitors hindered hydrogen evolution. Besides, with the increase of the P-Meth concentration, the corrosion current density reduced consistently. The similar trend was also observed with the test of P-Cys. The enhanced inhibition indicates that more inhibitors adsorbed onto the metal surface and the protective layer becoming tighter and reducing metal oxidization. Compared with β_c, β_a changed more dramatically, and therefore,

P-Meth and P-Cys mainly affected the anodic reactions. Moreover, the potentiodynamic polarization curves were parallel and similar, which suggests that these molecules inhibited metal corrosion by blocking the active sites on the metal surface. Besides, as illustrated in Tables S1 and S2, η_{IE} of the functionalized inhibitors displayed a considerable improvement comparing with the raw materials.

3.4. Adsorption isotherm

The adsorption isotherm is commonly employed in the assessment of the adsorption capacity of corrosion inhibitors on a metal surface. Although this analytical approach has prompted discussions regarding its reliability [44], it can be considered a semiquantitative indicator that provides insights into the Langmuir isothermal adsorption mechanisms [45–46]. Fig. 6 depicts the adsorption isotherms of P-Meth and P-Cys on the Q235 steel surface at 25°C. Notably, the adsorptions of P-Meth and P-Cys conformed to the Langmuir adsorption isotherms [47]:

$$\frac{c}{\theta} = \frac{1}{K_{ads}} + c \tag{9}$$

where c represents P-Meth or P-Cys concentration, θ denotes their surface coverage on the Q235 steel surface, and K_{ads} indicates the equilibrium adsorption constant.

Langmuir isotherms were plotted using EIS and potentiodynamic polarization data. The curves of c versus c/θ were all linear, and the correlation coefficient (R^2) was close to 1. The results showed a good correlation between corrosion inhibitor and Langmuir isotherm. Afterward, the standard free energy ΔG_{ads} was calculated using the following formula [47]:

$$\Delta G_{ads} = -RT\ln\left(10^6 K_{ads}\right) \tag{10}$$

where R and T represent a gas constant and the system temperature, respectively.

The ΔG_{ads} values of P-Meth and P-Cys were −34.18 and −34.32 kJ·mol^{-1} (Table S3), respectively. In general, when ΔG_{ads} is around −40 kJ·mol^{-1} or more negative, the process is classified as chemisorption, which indicates chemical bond formation between the organic corrosion inhibitor and metal surface. Conversely, when ΔG_{ads} is around −20 kJ·mol^{-1} or less negative, the process is considered to be physical adsorption, which involves electrostatic interactions between charged corrosion inhibitor molecules and the metal surface. ΔG_{ads} values in the range of −40 to −20 kJ·mol^{-1} suggest the coexistence of physical and chemical adsorption in the process [48–49]. Therefore, P-Meth and P-Cys were adsorbed onto the Q235 steel surface through mixed adsorptions, with chemical adsorption being the more favorable mechanism [38].

3.5. Quantum chemistry research

The molecular structures of P-Meth and P-Cys were optimized by density functional theory (DFT) method with B3LYP hybrid functional and 6-31g(d, p) basis set at Gaussian 09. Subsequently, the pre-optimized geometry was used to calculate single point energy with the B3LYP/6-311g(d, p) combined method. Then, the quantum chemical parameters of P-Meth and P-Cys, including atomic charges, frontier orbital energy (E_{HOMO}, E_{LUMO}), and Fukui functions were obtained. Based on the optimized structures and atomic property calculation results (Table S4), the frontier orbital occupancy diagrams were visualized to reveal the correlation between anticorrosion capability and molecular structure [50–52]. The HOMO and LUMO value surfaces of P-Meth and P-Cys are depicted in Fig. 7.

For P-Meth, the HOMO density distribution was mainly located on C–S bonds, and the LUMO was concentrated on the benzene ring, nitrogen, and oxygen contained in the unsaturated bonds. These features can also be found on the diagrams of P-Cys. In addition, the electron density on the nitrogen of P-Cys contributed to each frontier orbital interaction, and the hydrocarbon substituents on benzene slightly contributed to LUMO through hyperconjugation.

Table 4 shows the energies of HOMO and LUMO and the energy gap ($\Delta E = E_{LUMO} - E_{HOMO}$) [10]. In general, the E_{HOMO} is related to the molecular electron-donating capability, and the E_{LUMO} is connected to the electron-accepting capability. A low energy gap is assumed to indicate a desirable anticorrosion performance [53–57]. Table 4 shows the slightly lower energy gap of P-Meth than P-Cys. Therefore, given the calculated values, P-Meth may provide a relatively high IE, as suggested by experimental data.

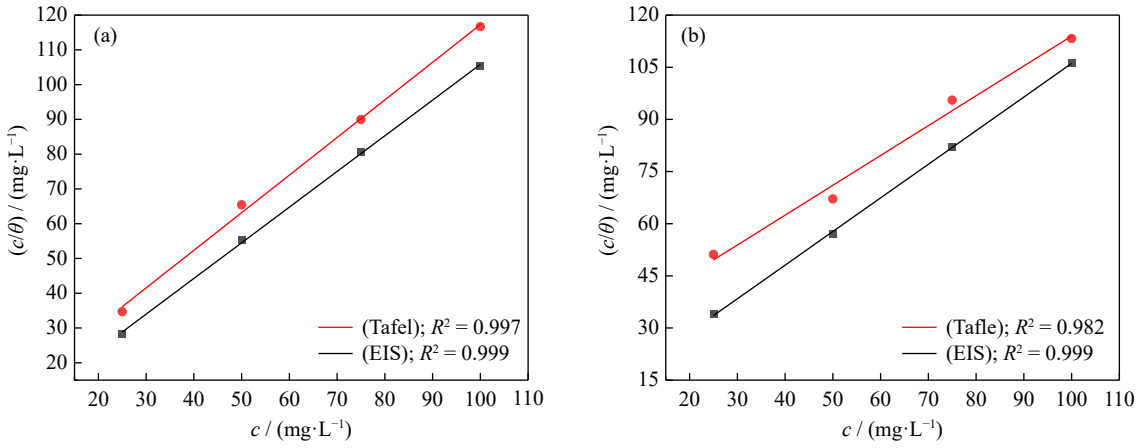

Fig. 6. Langmuir adsorption plots of Q235 steel in 1 M HCl containing different concentrations of (a) P-Meth and (b) P-Cys.

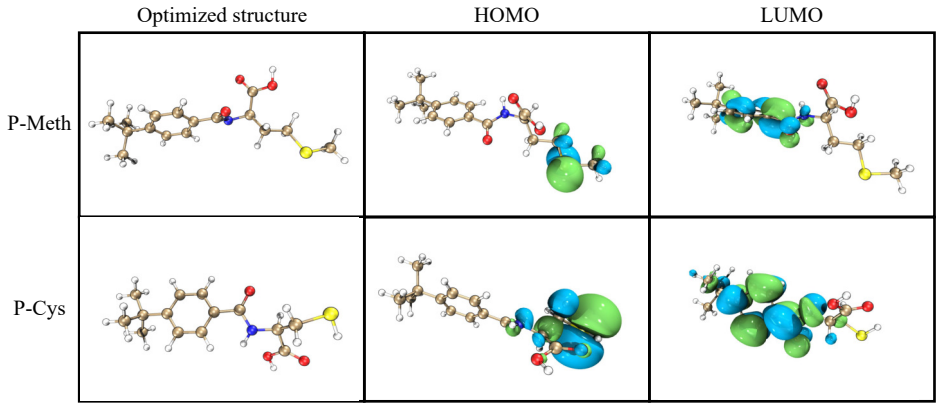

Fig. 7. Optimized geometric structure and frontier molecular density distributions of P-Meth and P-Cys (white ball, H; brown ball, C; red ball, O; blue ball, N; yellow ball, P).

Table 4. Calculated values of the relevant parameters of P-Meth and P-Cys

Inhibitor	E_{HOMO} / eV	E_{LUMO} / eV	ΔE / eV
P-Meth	−6.0300	−1.2816	4.7484
P-Cys	−6.4923	−1.3850	5.1073

The Fukui Indices of P-Meth and P-Cys were calculated using Hirshfield charges (Table S5) [57]. The Fukui function predicts the most electrophilic and nucleophilic sites of molecules. The large values of $f(+)$ demonstrated that heteroatoms accept electrons from steel surfaces to form a back-donating bond, and the larger values of $f(-)$ indicate that the oxygen atoms and carbons on benzene easily formed coordination bonds by donating electrons to the steel surface. Thus, the active sites on P-Meth and P-Cys corroborated the suggestion that the inhibitor molecules would form a protective layer on the iron surface.

3.6. MD simulation

To further study the active sites and adsorption mechanism of the two investigated amino acids, we used Forcite tools to simulate the interaction of inhibitor molecules on the steel surface and calculate the absorption (E_{ads}) and binding ($E_{binding}$) energies using the following equation [58–59]:

$$E_{ads} = E_{total} - (E_{surface+solution} + E_{inhibitor+solution}) + E_{solution} \quad (11)$$

$$E_{binding} = -E_{ads} \quad (12)$$

where E_{total} denotes the total potential energy of the system including iron crystal, 1 M muriatic solution ($500H_2O$, $9Cl^-$, and $9H^+$), and an inhibitor molecule. The simulation box was optimized before MD calculation. Fig. 8 shows the equilibrium snapshot of P-Meth and P-Cys over the Fe (100) surface from two perspectives. For both inhibitors, the moiety containing S atoms was more inclined to adsorb onto the iron surface, and the π bond on benzene tended to approach the steel surface. Thus, the inhibitor molecules covered the metal surface to the greatest extent, which enabled the improvement of the IE.

The energies were calculated using the vacuum and aqueous phases. The vacuum phase simulation was based on the MC approach and that for the aqueous phase on MD simulation (Fig. 8). Each method of simulation outputs 10 different equilibrium configurations consisting of 10 sets of energies. Their calculated average binding and adsorption energies are listed in Table 5. P-Meth exhibited a higher $E_{binding}$ than P-Cys, which means that the former may provide better adsorption onto the steel surface. In addition, the negative values of E_{ads} indicated the strong adsorption capability of both inhibitors. Compared with the two simulation environments, the adsorption behavior in the vacuum phase was inconsistent with those in acidic solutions. Therefore, the acidic environment had a great influence on IE.

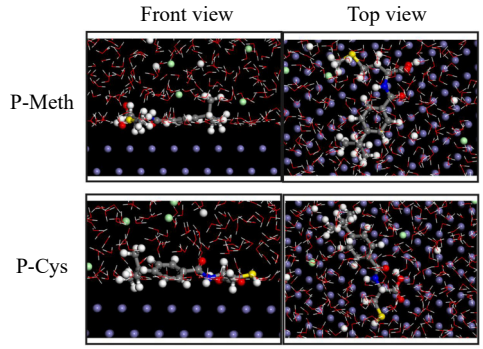

Fig. 8. Final snapshots of P-Meth and P-Cys through MD simulation from two perspectives (white ball, H; brown ball, C; red ball, O; blue ball, N; yellow ball, P; purple ball, Fe; green ball, Cl).

Table 5. Calculated binding and adsorption energies of P-Meth and P-Cys

System	$E_{binding}$ / (kJ·mol^{-1})	E_{ads} / (kJ·mol^{-1})
P-Meth + muriatic acid + Fe (110)	2688.19	−2688.19
P-Cys + muriatic acid + Fe (110)	2408.32	−2408.32
P-Meth + Fe (110)	2596.91	−2596.91
P-Cys + Fe (110)	1675.70	−1675.70

4. Conclusion

In this study, we demonstrated that the derivatives of p-tert-butyl benzoic acid with methionine or cysteine as the

functional groups led to the good corrosion inhibition effects to steels in strong acid conditions. All the weight loss analysis, morphology characterizations, EIS analysis, DFT, and MD results indicated that the better protective roles of P-Meth and P-Cys than those of p-tert-butyl benzoic acid. Specifically, 100 $mg \cdot L^{-1}$ P-Meth and P-Cys achieved inhibition efficiencies of 95.55% and 93.13%, respectively. Potentiodynamic polarization results indicate that amino acid derivatives acted as mixed-type corrosion inhibitors. EIS studies suggested that P-Meth and P-Cys formed a protective film through adsorption on the metal/solution interface, which increased the corrosion resistance of the steel sample. Moreover, the adsorption of these amino acid derivatives onto the metal surface conformed to the Langmuir isotherm. DFT calculations revealed the adsorption of the amino acid derivatives through interactions involving N and S atoms and the aromatic ring with the iron surface. MD simulations supported these findings, which confirm the superior adsorption capability of P-Meth over P-Cys. Future research should explore the alteration of other natural products to enhance anticorrosion and other desirable properties [60].

Acknowledgements

This work was supported by the Shenzhen Science and Technology Research Fund (Nos. JSGG20201103153807021, GXWD20220811173736002, and KCXFZ20230731094904009). We are also grateful to the Natural Science Foundation of Guangdong Province, China (No. 2021A1515110366), the National Natural Science Foundation of China (Nos. 22302048, 82204231, and 22004024), and the Shenzhen High Tech Zone Development Special Plan Innovation Platform Construction Project, China (No. 29853M-KCJ-2023-002-11).

Conflict of Interest

The authors declare no competing interests.

Supplementary Information

The online version contains supplementary material available at https://doi.org/10.1007/s12613-024-3011-8.

References

[1] L. Zhao, J.K. Wang, K. Chen, *et al*., Functionalized carbon dots for corrosion protection: Recent advances and future perspectives, *Int. J. Miner. Metall. Mater.*, 30(2023), No. 11, p. 2112.

[2] M.D. Alghamdi, Green nanomaterials and nanocomposites for corrosion inhibition applications, *Corros. Rev.*, 41(2023), No. 3, p. 349.

[3] H.Y. Wei, B. Heidarshenas, L.S. Zhou, G. Hussain, Q. Li, and K. Ostrikov, Green inhibitors for steel corrosion in acidic environment: State of art, *Mater. Today Sustain.*, 10(2020), art. No. 100044.

[4] M. Rbaa, F. Benhiba, R. Hssisou, *et al*., Green synthesis of novel carbohydrate polymer chitosan oligosaccharide grafted on d-glucose derivative as bio-based corrosion inhibitor, *J. Mol. Liq.*, 322(2021), art. No. 114549.

[5] D. Wang, J. Zhao, P. Claesson, *et al*., A strong enhancement of corrosion and wear resistance of polyurethane-based coating by chemically grafting of organosolv lignin, *Mater. Today Chem.*, 35(2024), art. No. 101833.

[6] Y. Zhang, C.P. Chen, H.Y. Tian, S.Q. Wang, C. Wen, and F. Chen, An ionic liquid-assisted strategy for enhanced anticorrosion of low-energy PEO coatings on magnesium–lithium alloy, *J. Magnes. Alloys*, 12(2024), No. 6, p. 2380.

[7] O.S. Michael, O. Borode, O.O. Alabi, K.K. Alaneme, and A.A. Adesoji, Evaluation of un-preprocessed expired piroxicam drug as corrosion inhibitor for mild steel in hydrochloric acid, *Int. J. Eng. Res. Afr.*, 61(2022), p. 29.

[8] Y. Zhang, S.T. Zhang, B.C. Tan, L. Guo, and H.T. Li, Solvothermal synthesis of functionalized carbon dots from amino acid as an eco-friendly corrosion inhibitor for copper in sulfuric acid solution, *J. Colloid Interface Sci.*, 604(2021), p. 1.

[9] Q.H. Zhang, B.S. Hou, Y.Y. Li, *et al*., Two amino acid derivatives as high efficient green inhibitors for the corrosion of carbon steel in CO_2-saturated formation water, *Corros. Sci.*, 189(2021), art. No. 109596.

[10] W.S. Guo, M. Talha, Y.H. Lin, Y.C. Ma, and X.W. Kong, Effect of phosphonate functional group on corrosion inhibition of imidazoline derivatives in acidic environment, *J. Colloid Interface Sci.*, 597(2021), p. 242.

[11] S.Z. Salleh, A.H. Yusoff, S.K. Zakaria, *et al*., Plant extracts as green corrosion inhibitor for ferrous metal alloys: A review, *J. Cleaner Prod.*, 304(2021), art. No. 127030.

[12] B.E. Ibrahimi, A. Jmiai, L. Bazzi, and S.E. Issami, Amino acids and their derivatives as corrosion inhibitors for metals and alloys, *Arab. J. Chem.*, 13(2020), No. 1, p. 740.

[13] D.Q. Zhang, Q.R. Cai, X.M. He, L.X. Gao, and G.D. Zhou, Inhibition effect of some amino acids on copper corrosion in HCl solution, *Mater. Chem. Phys.*, 112(2008), No. 2, p. 353.

[14] V. Shkirskiy, P. Keil, H. Hintze-Bruening, *et al*., The effects of l-cysteine on the inhibition and accelerated dissolution processes of zinc metal, *Corros. Sci.*, 100(2015), p. 101.

[15] W.N. Gong, X.S. Yin, Y. Liu, Y. Chen, and W.Z. Yang, 2-Amino-4-(4-methoxyphenyl)-thiazole as a novel corrosion inhibitor for mild steel in acidic medium, *Prog. Org. Coat.*, 126(2019), p. 150.

[16] X.C. Wang, N.J. Hu, J. Yang, *et al*., High-performance triboelectric nanogenerator based on ZrB_2/polydimethylsiloxane for metal corrosion protection, *Int. J. Miner. Metall. Mater.*, 30(2023), No. 10, p. 1957.

[17] X.J. Yang, J.H. Jia, Q. Li, *et al*., Stress-assisted corrosion mechanism of 3Ni steel by using gradient boosting decision tree machining learning method, *Int. J. Miner. Metall. Mater.*, 31(2024), No. 6, p. 1311.

[18] J.J. Fu, S.N. Li, Y. Wang, L.H. Cao, and L.D. Lu, Computational and electrochemical studies of some amino acid compounds as corrosion inhibitors for mild steel in hydrochloric acid solution, *J. Mater. Sci.*, 45(2010), No. 22, p. 6255.

[19] A. Fawzy, M. Abdallah, I.A. Zaafarany, S.A. Ahmed, and I.I. Althagafi, Thermodynamic, kinetic and mechanistic approach to the corrosion inhibition of carbon steel by new synthesized amino acids-based surfactants as green inhibitors in neutral and alkaline aqueous media, *J. Mol. Liq.*, 265(2018), p. 276.

[20] T.H. El-Mokadem, A.I. Hashem, N.E.A.A. El-Sattar, E.A. Dawood, and N.S. Abdelshafi, Green synthesis, electrochemical, DFT studies and MD simulation of novel synthesized thiourea derivatives on carbon steel corrosion inhibition in 1.0 M HCl, *J. Mol. Struct.*, 1274(2023), art. No. 134567.

[21] M.A. Deyab, J.M. AlGhamdi, M.M. Abdeen, *et al*., Chemical, electrochemical, and quantum investigation into the use of an organophosphorus derivative to inhibit copper corrosion in acid-

ic environments, *Sci. Rep.*, 14(2024), No. 1, art. No. 11395.
[22] V. Srivastava, J. Haque, C. Verma, *et al*., Amino acid based imidazolium zwitterions as novel and green corrosion inhibitors for mild steel: Experimental, DFT and MD studies, *J. Mol. Liq.*, 244(2017), p. 340.
[23] D.S. Chauhan, M.A. Quraishi, V. Srivastava, J. Haque, and B.E. ibrahimi, Virgin and chemically functionalized amino acids as green corrosion inhibitors: Influence of molecular structure through experimental and in silico studies, *J. Mol. Struct.*, 1226(2021), art. No. 129259.
[24] H. Cang, Z.H. Fei, W.Y. Shi, and Q. Xu, Experimental and theoretical study for corrosion inhibition of mild steel by L-cysteine, *Int. J. Electrochem. Sci.*, 7(2012), No. 10, p. 10121.
[25] W.W. Zhang, Y.X. Zhang, B.Z. Li, *et al*., High-performance corrosion resistance of chemically-reinforced chitosan as eco-friendly inhibitor for mild steel, *Bioelectrochemistry*, 150(2023), art. No. 108330.
[26] W.W. Zhang, C.Y. Li, W.J. Wang, *et al*., Laminarin and sodium molybdate as efficient sustainable inhibitor for Q235 steel in sodium chloride solution, *Colloids Surf. A*, 637(2022), art. No. 128199.
[27] T. Lu and F.W. Chen, Multiwfn: A multifunctional wavefunction analyzer, *J. Comput. Chem.*, 33(2012), No. 5, p. 580.
[28] A. Chaouiki, F. Hazmatulhaq, D.I. Han, A.H. Al-Moubaraki, M. Bakhouch, and Y.G. Ko, Predicting the interaction between organic layer and metal substrate through DFTB and electrochemical approach for excellent corrosion protection, *J. Ind. Eng. Chem.*, 114(2022), p. 190.
[29] A. Dehghani, G. Bahlakeh, B. Ramezanzadeh, A.H.J. Mofidabadi, and A.H. Mostafatabar, Benzimidazole loaded β-cyclodextrin as a novel anti-corrosion system; coupled experimental/computational assessments, *J. Colloid Interface Sci.*, 603(2021), p. 716.
[30] M. Chafiq, A. Chaouiki, M.R. Albayati, *et al*., Unveiled understanding on corrosion inhibition mechanisms of hydrazone derivatives based on naproxen for mild steel in HCl: A joint experimental/theoretical study, *J. Mol. Liq.*, 320(2020), art. No. 114442.
[31] E. Gutiérrez, J.A. Rodríguez, J. Cruz-Borbolla, J.G. Alvarado-Rodríguez, and P. Thangarasu, Development of a predictive model for corrosion inhibition of carbon steel by imidazole and benzimidazole derivatives, *Corros. Sci.*, 108(2016), p. 23.
[32] H.X. Zhao, X.H. Zhang, L. Ji, H.X. Hu, and Q.S. Li, Quantitative structure–activity relationship model for amino acids as corrosion inhibitors based on the support vector machine and molecular design, *Corros. Sci.*, 83(2014), p. 261.
[33] A. Singh, K.R. Ansari, D.S. Chauhan, M.A. Quraishi, H. Lgaz, and I.M. Chung, Comprehensive investigation of steel corrosion inhibition at macro/micro level by ecofriendly green corrosion inhibitor in 15% HCl medium, *J. Colloid Interface Sci.*, 560(2020), p. 225.
[34] B.C. Tan, J.H. He, S.T. Zhang, *et al*., Insight into anti-corrosion nature of Betel leaves water extracts as the novel and eco-friendly inhibitors, *J. Colloid Interface Sci.*, 585(2021), p. 287.
[35] A. Singh, K.R. Ansari, M.A. Quraishi, S. Kaya, and S. Erkan, Chemically modified guar gum and ethyl acrylate composite as a new corrosion inhibitor for reduction in hydrogen evolution and tubular steel corrosion protection in acidic environment, *Int. J. Hydrogen Energy*, 46(2021), No. 14, p. 9452.
[36] S.M. Tawfik, Alginate surfactant derivatives as an ecofriendly corrosion inhibitor for carbon steel in acidic environments, *RSC Adv.*, 5(2015), No. 126, p. 104535.
[37] M.A. Hegazy, A.M. Hasan, M.M. Emara, M.F. Bakr, and A.H. Youssef, Evaluating four synthesized Schiff bases as corrosion inhibitors on the carbon steel in 1M hydrochloric acid, *Corros. Sci.*, 65(2012), p. 67.
[38] M.S.S. Adam, H.M.A. El-Lateef, and K.A. Soliman, Anionic oxide-vanadium Schiff base amino acid complexes as potent inhibitors and as effective catalysts for sulfides oxidation: Experimental studies complemented with quantum chemical calculations, *J. Mol. Liq.*, 250(2018), p. 307.
[39] Z. Zhang, N.C. Tian, L.Z. Zhang, and L. Wu, Inhibition of the corrosion of carbon steel in HCl solution by methionine and its derivatives, *Corros. Sci.*, 98(2015), p. 438.
[40] J.H. Zhang, X.J. Luo, Y.Y. Ding, L.Q. Chang, and C.F. Dong, Effect of bipolar-plates design on corrosion, mass and heat transfer in proton-exchange membrane fuel cells and water electrolyzers: A review, *Int. J. Miner. Metall. Mater.*, 31(2024), No. 7, p. 1599.
[41] J. Haque, V. Srivastava, M.A. Quraishi, D.S. Chauhan, H. Lgaz, and I.M. Chung, Polar group substituted imidazolium zwitterions as eco-friendly corrosion inhibitors for mild steel in acid solution, *Corros. Sci.*, 172(2020), art. No. 108665.
[42] A.O. Yüce, B.D. Mert, G. Kardaş, and B. Yazıcı, Electrochemical and quantum chemical studies of 2-amino-4-methylthiazole as corrosion inhibitor for mild steel in HCl solution, *Corros. Sci.*, 83(2014), p. 310.
[43] H. Ashassi-Sorkhabi, M.R. Majidi, and K. Seyyedi, Investigation of inhibition effect of some amino acids against steel corrosion in HCl solution, *Appl. Surf. Sci.*, 225(2004), No. 1-4, p. 176.
[44] M.S. Walczak, P. Morales-Gil, and R. Lindsay, Determining Gibbs energies of adsorption from corrosion inhibition efficiencies: Is it a reliable approach?, *Corros. Sci.*, 155(2019), p. 182.
[45] A.A. Mansour, C. Hejjaj, F.Z. Thari, *et al*., Interfacial phenomena and surface protection of N80-carbon steel in acidic environments using thiazolidinediones: An experimental and computational analysis, *Colloids Surf. A*, 677(2023), art. No. 132415.
[46] A. Kokalj, A general-purpose adsorption isotherm for improved estimation of standard adsorption free energy, *Corros. Sci.*, 217(2023), art. No. 111124.
[47] A. Mittal, L. Kurup, and J. Mittal, Freundlich and Langmuir adsorption isotherms and kinetics for the removal of Tartrazine from aqueous solutions using hen feathers, *J. Hazard. Mater.*, 146(2007), No. 1-2, p. 243.
[48] A.K. Singh, B. Chugh, S.K. Saha, *et al*., Evaluation of anti-corrosion performance of an expired semi synthetic antibiotic cefdinir for mild steel in 1 M HCl medium: An experimental and theoretical study, *Results Phys.*, 14(2019), art. No. 102383.
[49] A. Kosari, M.H. Moayed, A. Davoodi, *et al*., Electrochemical and quantum chemical assessment of two organic compounds from pyridine derivatives as corrosion inhibitors for mild steel in HCl solution under stagnant condition and hydrodynamic flow, *Corros. Sci.*, 78(2014), p. 138.
[50] L.O. Olasunkanmi, I.B. Obot, M.M. Kabanda, and E.E. Ebenso, Some quinoxalin-6-yl derivatives as corrosion inhibitors for mild steel in hydrochloric acid: Experimental and theoretical studies, *J. Phys. Chem. C*, 119(2015), No. 28, p. 16004.
[51] H. Ashassi-Sorkhabi, S. Moradi-Alavian, R. Jafari, A. Kazempour, and E. Asghari, Effect of amino acids and montmorillonite nanoparticles on improving the corrosion protection characteristics of hybrid sol-gel coating applied on AZ91 Mg alloy, *Mater. Chem. Phys.*, 225(2019), p. 298.
[52] R. Hernández-Bravo, A.D. Miranda, J.G. Parra, J.M. Alvarado-Orozco, J.M. Domínguez-Esquivel, and V. Mujica, Experimental and theoretical study on the effectiveness of ionic liquids as corrosion inhibitors, *Comput. Theor. Chem.*, 1210(2022), art. No. 113640.
[53] T.B. Zhang, W.F. Jiang, H.L. Wang, and S.F. Zhang, Synthesis and localized inhibition behaviour of new triazine-methionine corrosion inhibitor in 1 M HCl for 2024-T3 aluminium alloy, *Mater. Chem. Phys.*, 237(2019), art. No. 121866.
[54] J. Haque, V. Srivastava, C. Verma, H. Lgaz, R. Salghi, and M.A. Quraishi, N-methyl-N, N, N-trioctylammonium chloride

as a novel and green corrosion inhibitor for mild steel in an acid chloride medium: Electrochemical, DFT and MD studies, *New J. Chem.*, 41(2017), No. 22, p. 13647.

[55] J. Haque, V. Srivastava, C. Verma, and M.A. Quraishi, Experimental and quantum chemical analysis of 2-amino-3-((4-((S)-2-amino-2-carboxyethyl)-1H-imidazol-2-yl)thio) propionic acid as new and green corrosion inhibitor for mild steel in 1M hydrochloric acid solution, *J. Mol. Liq.*, 225(2017), p. 848.

[56] W.W. Zhang, H.J. Li, L.W. Chen, *et al*., Performance and mechanism of a composite scaling-corrosion inhibitor used in seawater: 10-Methylacridinium iodide and sodium citrate, *Desalination*, 486(2020), art. No. 114482.

[57] H.S. Sujatha and M.Lavanya, An insight to HOMO LUMO aspects in corrosion applications, *Can. Metall. Q.*, 62(2023), No. 4, p. 761.

[58] M. Xiao and T. Lu, Generalized charge decomposition analysis (GCDA) method, *J. Adv. Phys. Chem.*, 4(2015), No. 4, p. 111.

[59] R. Hsissou, S. Abbout, R. Seghiri, *et al*., Evaluation of corrosion inhibition performance of phosphorus polymer for carbon steel in [1 M] HCl: Computational studies (DFT, MC and MD simulations), *J. Mater. Res. Technol.*, 9(2020), No. 3, p. 2691.

[60] S.K. Saha, A. Dutta, P. Ghosh, D. Sukul, and P. Banerjee, Novel Schiff-base molecules as efficient corrosion inhibitors for mild steel surface in 1 M HCl medium: Experimental and theoretical approach, *Phys. Chem. Chem. Phys.*, 18(2016), No. 27, p. 17898.